Direction-Controlled Light-Driven Movement of Microribbons

Yifan Zhang, Cheng Peng, Bin Cui, Zhengfei Wang, Xibin Pang, Renmin Ma, Feng Liu, Yanke Che,* and Jincai Zhao*

Molecular crystals or polymer films composed of photoresponsive molecular motors or components have attracted substantial attention because of their potential applications in actuators and artificial muscles, among others.[1–18] However, although some photoinduced morphological changes resulting from the collective transmission of single-molecule motions enable the movement of microscale objects loaded onto their surfaces,[8,13,19] the ability of molecular crystals or polymer films to transmit molecular motion to direction-controlled autonomous movements remains a great challenge. We recently reported that layered microribbons assembled from asymmetric perylene diimide (PDI) molecules underwent a lateral or longitudinal morphological change under scanning laser irradiation.[20] The photoexcited intermolecular distortions generate large morphological changes. This motivated us to investigate the possibility of applying photoexcited nonbonded distortions to generate the direction-controlled autonomous movements of the microribbons on specific substrates.

Here, we report novel direction-controlled movements of microribbons self-assembled from PDI molecules on various hydrophobic surfaces (including octadecyltriethoxysilane (OTS)-, 1H,1H,2H,2H-Perfluorodecyltriethoxysilane-, and Scotch tape-modified glass slide) under scanning laser irradiation. We develop a "dynamic exciton charge model (DECM)" to elucidate the underlying mechanism. It is demonstrated that the spatial release of instantaneous excitonic dipole–dipole or quadrupole–quadrupole interactions of the photoexcited π-stacks is related to the molecular intrinsic structure and packing geometry, which induces the directional intermolecular distortion, and thus the different movement directions of the resulting microribbons, e.g., parallel or normal to the long axis of the microribbon. More importantly, through varying the side chains of the building block, which enables the modulation of the diagonal direction of the π-stacks and thus the diagonal photoexcited distortion relative to the long axis of the microribbon, angular movements of the resulting microribbons were achieved. Our findings provide an innovative strategy for the design of microscale systems capable of continuous and directional movement driven by light.

We envision that the microribbon assembled from **1** (**Figure 1**) may make a transverse movement on a less resistant substrate if the irradiation intensity is reduced to avoid a morphological change between stacking layers[20] but is still sufficient to induce the intermolecular distortion on the surface of the microribbon. Indeed, as shown in Figure 1a and Movie S1 in the Supporting Information, when irradiated with a 488 nm scanning laser (54 W mm^{-2}, 4 µs per pixel, 600 × 300 pixels per frame), the microribbon from **1** moved in the direction normal to the long axis of the microribbon on an OTS-modified glass slide. More than 10 microribbons assembled from **1** were tested under identical conditions, and the movement speed was similar for microribbons of the same length under identical irradiation conditions. The typical speed of a microribbon with a length of 50 µm and a width of 1 µm was ≈0.5 µm min^{-1} when irradiated with a 488 nm scanning laser (54 W mm^{-2}, 4 µs per pixel, 600 × 300 pixels per frame) (Figure 1b). Upon a further increase of the irradiation intensity, the microribbon assembled from **1** moved faster but concomitantly began to expand laterally. Notably, the microribbons were observed to move to the right and the left randomly, analogous to the sliding out of the microribbons in both directions on the pristine glass slide.[20]

We envision that such transverse moving direction is dependent on molecular packing within the microribbon and the movements in different direction (e.g., longitudinal movement) may be achieved on the microribbons with distinct molecular packing geometry. To this end, we synthesis a symmetric PDI molecule **2**, which is expected to form microribbons with different molecular packing. Well-defined microribbons assembled from **2**, analogous to those assembled from **1**, were clearly revealed by the scanning electron microscopy (SEM) images (**Figure 2**a,b). The selected-area electron diffraction pattern (SAED) and X-ray diffraction (XRD) results (Figure S1, Supporting Information) revealed that the molecular organization of **2** within the microribbon is same to that observed in the bulk crystal.[21] The molecular packing of **2**

Dr. Y. Zhang, Dr. C. Peng, Dr. X. Pang, Prof. Y. Che, Prof. J. Zhao
Beijing National Laboratory for Molecular Sciences
Key Laboratory of Photochemistry
Institute of Chemistry
Chinese Academy of Sciences
Beijing 100190, China
E-mail: ykche@iccas.ac.cn
Dr. Y. Zhang, Dr. C. Peng, Dr. X. Pang, Prof. Y. Che, Prof. J. Zhao
University of Chinese Academy of Sciences
Beijing 100049, China
Dr. B. Cui, Dr. Z. Wang, Prof. F. Liu
Department of Materials Science and Engineering
University of Utah
Salt Lake City
UT 84112, USA
E-mail: fliu@eng.utah.edu
Prof. R. Ma
State Key Lab for Mesoscopic Physics and School of Physics
Peking University
Beijing 100871, China

DOI: 10.1002/adma.201602411

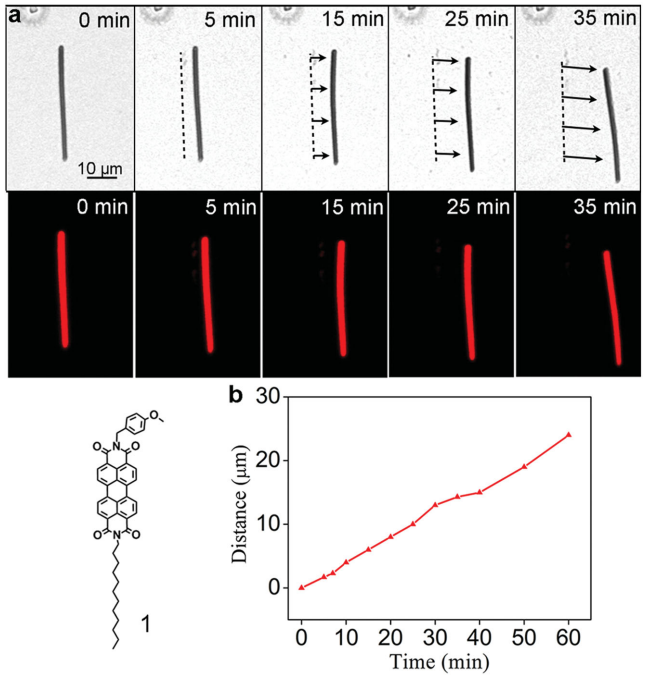

Figure 1. a) Optical microscopy images (top: bright-field images; bottom: fluorescence images) of a typical microribbon assembled from **1** showing translational movement nearly normal to its long axis under laser irradiation (54 W mm^{-2}, 4 μs per pixel, 600 × 300 pixels per frame). b) Moving distance of the same microribbon assembled from **1** as a function of time.

in the microribbons, as viewed from different faces, was presented in Figure S1 in the Supporting Information. A small longitudinal offset between neighboring molecules of **2** gives rise to a strong π-overlap along the microribbon axis as evidenced by the absorption spectrum (Figure S2, Supporting Information) where the broad absorption bandwidth centered at 690 nm was observed. Furthermore, such longitudinal slipping resulted in the absorption and emission polarization parallel to the microribbon axis (Figure S3, Supporting Information),[22] which is in sharp contrast to the transversal packing of **1** microribbon (Figure S4, Supporting Information) that generated the absorption and emission polarization normal to the long axis of **1** microribbon (Figure S3, Supporting Information).[22] When excited by laser (e.g., at 488 nm), the interaction of excited **2** molecules (i.e., excitonic quadrupole–quadrupole interaction) within the π-stacks is expected to generate the π-stacking distortion parallel to the microribbon axis. Indeed, the microribbon assembled from **2** moved along the microribbon axis rather than normal to the microribbon axis, as shown in Figure 2c and Movie S2 in the Supporting Information. When several microribbons were irradiated concurrently, all exhibited longitudinal movement (Figure 2d), indicative of the reproducibility of the movement. The typical movement speed was measured to be ≈2 μm min^{-1} for a microribbon assembled from **2** with a length of 80 μm and a width of 0.8 μm under scanning laser irradiation (Figure 2c,e). The microribbons assembled from **2** are relatively photostable; thus, their movement speed can be measured as a function of the irradiation intensity. As shown in Figure 2f, the movement speed of the microribbon linearly increased with increasing laser intensity. Notably, no

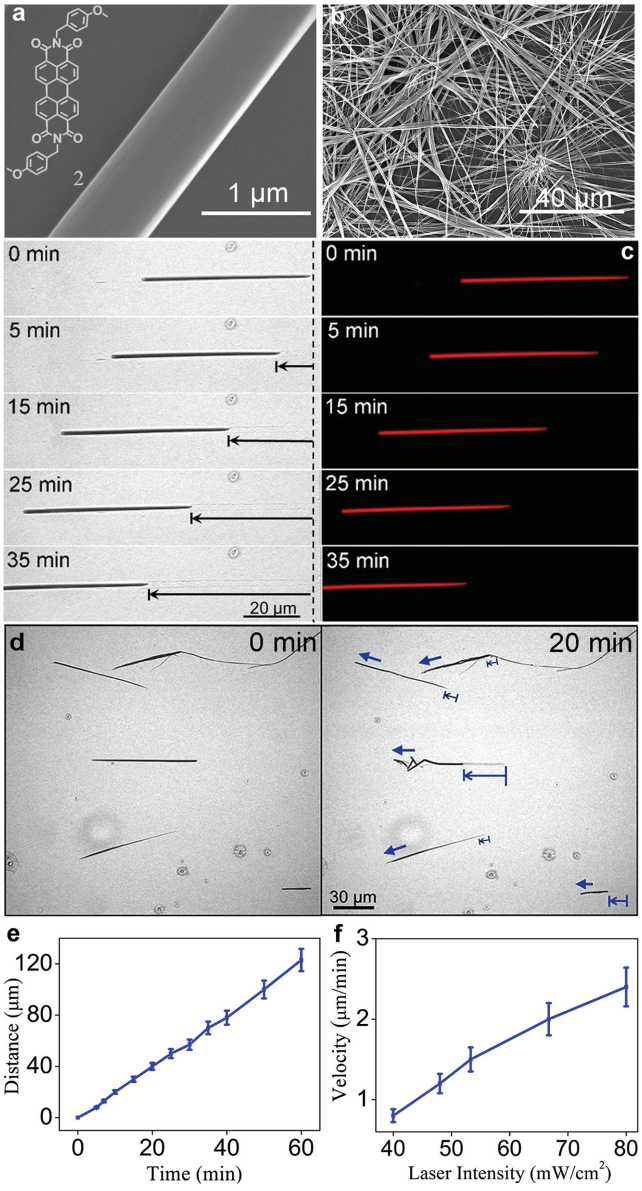

Figure 2. a) A magnified SEM image of a single microribbon assembled from molecule **2**. b) SEM image of bundles of microribbons. c) Optical microscopy images (left: bright-field images; right: fluorescence images) of a typical microribbon from **2** showing translational movement along its long axis under scanning laser irradiation (488 nm, 108 W mm^{-2}, 4 μs per pixel, 800 × 300 pixels per frame). d) The movement of a couple of microribbons from **2** under scanning laser irradiation (488 nm, 108 W mm^{-2}, 4 μm per pixel, 800 × 800 pixels per frame). All of microribbons moved away from their original position after 20 min of scanning irradiation. e) Moving distance of the microribbons as a function of time (more than 5 microribbons were tested). f) The moving velocity of microribbon assembled from molecule **2** as a function of laser intensity (488 nm, 4 μs per pixel, 800 × 300 pixels per frame).

discernible movement for the microribbon assembled from **2** was observed when the irradiation intensity was less than 54 W mm^{-2}, indicative of the existence of a barrier threshold for the movement. In addition, no motion of the microribbons assembled from molecules **1** and **2** occurred on pristine glass

slide, indicating that the substrate surfaces are critical to the microribbon movement. We compared the movement velocity of the same microribbons on different surfaces (Table S1, Supporting Information). The microribbons exhibited a relatively fast movement on the hydrophobic surfaces and almost no movement on the hydrophilic surfaces under identical irradiation conditions. This suggests that the interactions between substrate surfaces and the bottom surface of the microribbons are different, which thereby created different resistance for the movement of the microribbon and in turn affected the movement rate. We used the OTS-modified glass slide as the substrate in the following experiments unless otherwise specified.

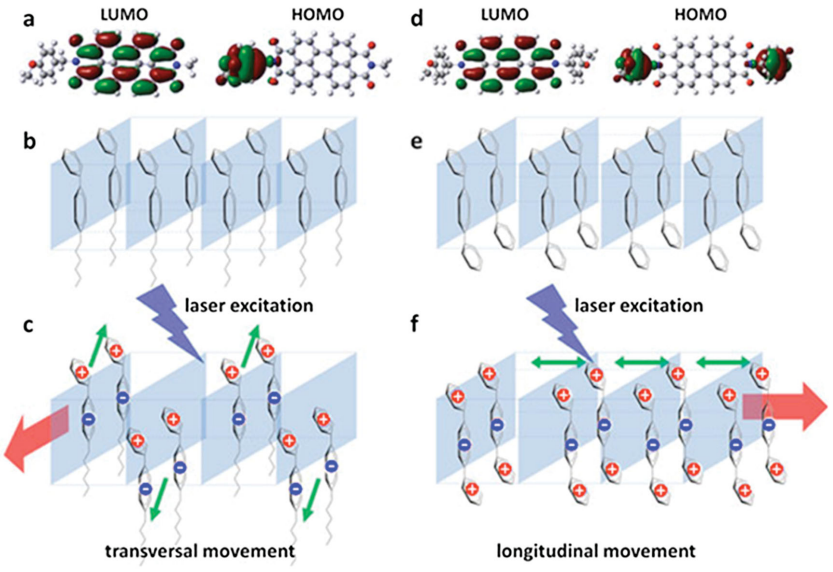

Figure 3. a) HOMO and LOMO charge distribution of **1**. b) Structural arrangement of the microribbon from **1**. c) Photoinduced charge distribution, 1 molecular motion, and microribbon movement. d) HOMO and LOMO charge distribution of **2**. e) Structural arrangement of the microribbon from **2**. f) Photoinduced charge distribution, **2** molecular motion, and microribbon movement.

To confirm the photoinduced intermolecular distortion, the fluorescent switching dynamics, which reveal the behavior of the excited-state nonbonded distortion,[23] was studied by time-resolved fluorescence spectroscopy. Spectral trajectories measured by irradiating one end of microribbons of **1** and **2** with a nanosecond pulsed laser (532 nm, 12 μW pulse^{-1}) and collected by the spectrometer with a resolution of 8 ms show that the π-stacking emission spectrum periodically changed within certain timescales (Figures S5 and S6, Supporting Information). Although observed spectral changes are minor (the time resolution of fluorescence spectroscopy used in this work is not high enough compared to the fast dynamic π-stacking distortion process), the statistical emission band of the microribbon from **1** and **2** did show slightly blueshifted and redshifted in the beginning, respectively, and then restored to its original position (Figures S5 and S6, Supporting Information) within ≈24 ms, indicating that the system rapidly and periodically switched from the photoinduced intermolecular distortion to the original π-stacking structure. These switching dynamics within the π-stacks are comparable to those observed during the excited-state nonbonded distortion of locked PDI oligomers.[23] To further understand how the photoinduced intermolecular distortion induces the directional movements of the microribbons, we propose a DECM model based on theoretical calculations of photoinduced intermolecular excitonic dipole–dipole or quadrupole–quadrupole interactions that distinguish the different movement of microribbons from **1** versus **2**. From the calculations of HOMO_LOMO states, as shown in **Figure 3**, the main difference between **1** and **2** is that the photoexcitation creates a dipole in **1** but quadrupole in **2**, due to their different molecular structure. Consequently, the distortion of microribbons is driven by releasing instantaneous excitonic dipole–dipole or quadrupole–quadrupole interactions, which create certain preferred internal relative motions in between the molecules that in turn translate into an overall movement of microribbon along a preferred direction. Applying the DECM, the preferred molecular motion is determined, as shown in Figure 3. Using the experimentally measured crystalline structures as input (the molecular packing of **1** in the microribbons was shown in Figure S4, Supporting Information), we construct a molecular array to represent the microribbons from **1** and **2** in Figure 3, respectively. Upon photoexcitation, a charge-transfer bound electron–hole pair (exciton) is created on each molecule with the electron (negative charge) and hole (positive charge) placed on different aromatic rings within the molecule, which creates the dipole in **1** (Figure 3c) but quadrupole in **2** (Figure 3f). For **1**, by minimizing the dipole–dipole interactions, we found a shearing motion between the neighboring **1** molecules, as indicated by green arrows in Figure 3c. This shearing motion, having a larger vertical component than the horizontal component, is possibly facilitated by the tails of alkane chains. With the dipoles instantaneously appear by photo excitation and disappear by exciton decay, there will be a collective back-and-forth shearing motion in between many molecules, which translate to an overall transversal movement of the **1** microribbon, as indicated by the red arrow in Figure 3c. In contrast, the motion of **2** microribbon is driven by releasing instantaneous excitonic quadrupole–quadrupole interactions along π-stacks. With the light-induced instantaneous quadrupoles dynamically appear and disappear, there will be a collective lateral breathing motion (expansion and contraction) in between many molecules, which translate to an overall longitudinal movement of the **2** microribbon, as indicated by the red arrow in Figure 3f. Furthermore, by calculating the forces along the motion direction, the speed of **2** microribbon is expected to be faster than that of **1** microribbon, consistent with experimental results.

To gain insight into how the instantaneous photoinduced intermolecular distortions translate into an overall movement of the microribbons, we explored the role of the scanning laser in the resulting movements. The necessity of the scanning laser was proved by the failure of the microribbons from **1** or **2** to move under constant laser irradiation. We observed that

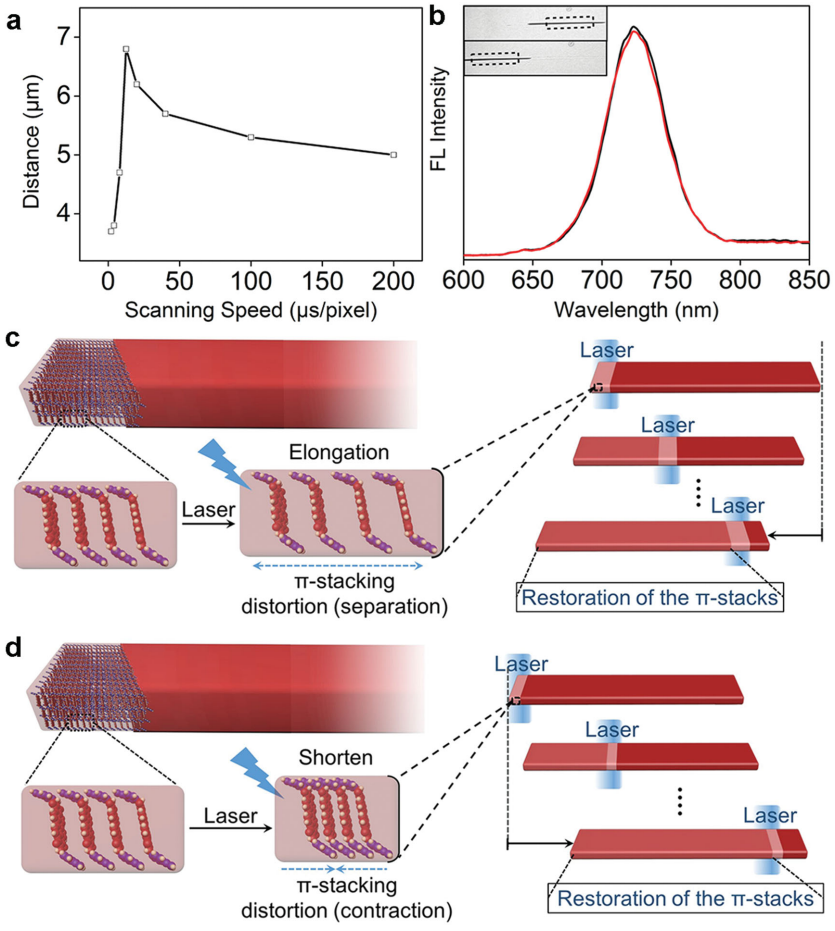

Figure 4. a) Moving distance of a typical microribbon from **2** (10 μm in length and 1 μm in width) after 200 scanning frames as a function of laser scanning speed. b) Fluorescence spectra of a microribbon assembled from **2** recorded at the same position before (black) and after (red) movement. c,d) Schematic representation of the directional movement process excited by scanning laser. The photoexcited separation (c) or contraction (d) of π-stacks and the followed restoration of the π-stacks would occur point by point along the microribbon upon a scanning laser. The spatially dynamic variance between the photoexcited distortion and restoration would create a certain displacement after each scanning circle.

the microribbons were damaged, rather than underwent movement when the high intensity of the constant laser irradiation was applied. Under scanning laser irradiation, the photoexcited distortion (separation or contraction) and the followed restoration of the π-stacks would occur point by point along the microribbon, somehow like earthworm movements; the spatially dynamic variance between the photoexcited distortion and restoration would create a certain displacement after each scanning circle. For better understanding of the whole process, an illustration was performed in **Figure 4**c,d. We anticipated that the laser scanning speed could modulate the spatial dynamic variance of the photoexcited distortion and the followed restoration of the π-stacks and in turn influence the movement velocity of the microribbons. To truly reflect the dependence of the movement velocity on the scanning irradiation, we compared the movement distance of the same microribbon from **2** after 200 scanning frames (i.e., the same scanning circles). As typically shown in Figure 4a, the movement velocity of the microribbons from **2** was indeed dependent on the laser-scanning speed. The moved distance of the **2** microribbon after 200 scanning frames initially increased quickly with the increasing scanning speed from 2 to 12.5 μs per pixel and then decreased with the further increasing scanning speed, suggesting the existence of an optimal dynamics of the photoinduced distortion and restoration for the microribbon movement. Notably, the fluorescence spectra and intensity of the microribbons remained unchanged after the movement (Figure 4b), indicating the reversibility of the nonbonded distortion that enables the continuous movements of the assembled microribbons.

We also exclude the possibility of forces induced motion from other sources. First, a temperature gradient along the thickness direction of the microribbon could be set up and cause a gradient stress in the thickness direction. However, such a gradient stress should only cause out-of-plane morphological changes (analogous to those induced by surface stress anisotropy generated by the photocyclodimerization,[6,7] photoisomerization,[24] polymerization,[12,25] or drying[26,27]), rather than result in directional movements. Likewise, the gradient photoexcited nonbonded distortion along the microribbon thickness direction, which results from the high absorption of the PDI molecules in the microribbon, could create a gradient stress along the thickness direction. However, such a gradient stress should also cause out-of-plane morphological changes. In addition, the radiation pressure that corresponds to a force in the light propagation direction[28] could be also set up to be along the microribbon thickness because the microribbons were irradiated from the bottom surface. Again, this vertical force cannot cause translational movements. Furthermore, the failure of the movements of microribbons assemble from molecules **6** and **7** (see Supporting Information) as control experiments suggested that forces along the thickness direction (that should be also set up in these microribbon under identical conditions) could not be the driving force for the resulting movement of the microribbons. Second, a temperature gradient spatially along the long axis of the microribbon (the scanning irradiation direction was consistent with the long axis) could be also set up and cause a gradient stress in the microribbon long axis. However, because photothermal effects work relatively slower,[29,30] the decreased laser scanning speed should increase temperature-driven effect and thereby speed up the movements. However, on the contrary, the movement speed of the examined microribbon (Figure 4a) decreased with the decreasing laser-scanning speed (more than 12.5 μs per pixel), thereby ruling out the possibility that a temperature gradient spatially along the long axis of the

microribbon induced the movements. Finally, the scanning irradiation of the microribbons from **1** by a 635 nm laser (the **1** microribbons have negligible absorption at 635 nm, Figure S2, Supporting Information) could not result in the microribbon movement, ruling out the possibility that the optical force from light scattering could create the movement. In addition, the scanning irradiation of the **2** microribbons by 515 and 635 nm lasers (**2** microribbons have relatively strong absorption at 515 and 635 nm, Figure S2, Supporting Information) also resulted in the similar translational movements, suggesting that the larger dipole moment possibly induced by a 488 nm laser is not necessary.

The observation of directional translational movements of the microribbons assembled from **1** and **2** motivated us to further explore achieving angular movements of microribbons. If the diagonal direction of the photoinduced intermolecular distortion relative to the long axis of the microribbon can be achieved, angular movements of the resulting microribbons could be created. To this end, two PDI molecules, **3** and **4**, which bear 3,5-dimethoxy and 2,3-dimethoxy substituents on their phenyl groups, respectively, were synthesized and self-assembled into microribbons. SAED and XRD results (Figures S7 and S8, Supporting Information) reveal that the molecular organization of **3** and **4** within π-stacks is similar to that observed in the microribbon from **2**. Therefore, the photoinduced distortions of **3** and **4** π-stacks should be also similar to that of **2** microribbon, which results from instantaneous quadrupole–quadrupole interactions. However, distinct from that of **2** that has no angular offset relative to the microribbon axis (Figure S1, Supporting Information), the π-stacking direction of **3** and **4** had an angular offset of 5° and 10°, respectively, relative to the long axis of the microribbon (Figures S7 and S8, Supporting Information). Consequently, under scanning laser irradiation, a microribbon from **3** exhibited an angular movement across the substrate surface accompanied with a warp of the microribbon, as illustrated in **Figure 5**a and Movie S3, Supporting Information. We postulate that the warp of the microribbon resulted from the uneven velocity of the relatively long microribbon, not from its softness. To support this hypothesis, a shorter microribbon from **3** was studied under identical conditions. As shown in Figure 5b, the short microribbon exhibited only an angular movement without the shape change. To further prove the microribbon from **3** is not soft, the differential scanning calorimetry measurement was performed and the endothermic peak at 191 °C, assignable to the melt of the microribbon, was observed (Figure S9, Supporting Information); this phase transition temperature is much higher than that of **1** microribbons (138 °C), suggesting molecule **3** has stronger molecular packing than **1**. Notably, the microribbon from **4** with a larger angular offset exhibited a rotational movement (i.e., a stronger angular movement) (Figure 5c and Movie S4, Supporting Information), because of the larger offset between the diagonal direction of its π-stacking relative to the long axis of the microribbon. Interestingly, the microribbon from **4** exhibited the contrary rotational movements upon irradiation of different surfaces (bottom or top) of the microribbons (Movies S5 and S6, Supporting Information), indicating that the photoinduced rotation direction is determined by the diagonal direction of the π-stacking in the microribbon relative

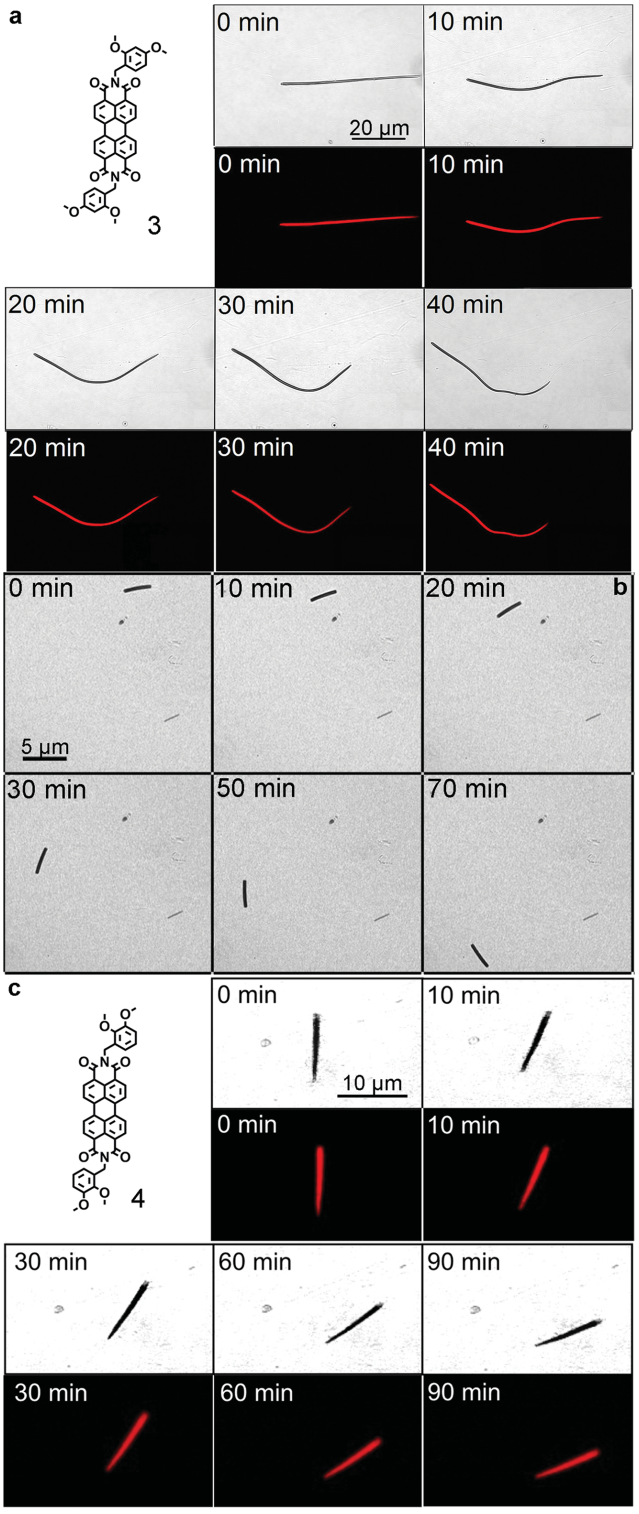

Figure 5. a) An angular movement of a long microribbon (≈50 μm) assembled from **3** (top: bright-field images; bottom, fluorescence images) under scanning laser irradiation (488 nm, 108 W mm^{-2}, 4 μs per pixel, 700 × 350 pixels per frame). b) An angular movement of a short microribbon (5 μm) assembled from **3** under scanning laser irradiation (488 nm, 108 W mm^{-2}, 4 μs per pixel, 400 × 400 pixels per frame). c) A rotational movement of the microribbon assembled from **4** under scanning laser irradiation (488 nm, 108 W mm^{-2}, 4 μs per pixel, 300 × 250 pixels per frame).

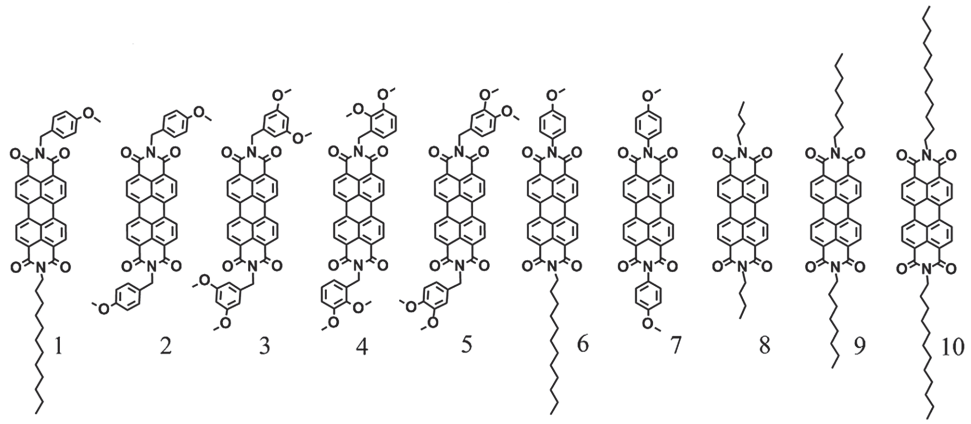

Figure 6. Chemical structures of PDI derivatives.

to its long axis. More interestingly, the microribbons from **3** and **4** with one end hung on a copper grid also exhibited a warping movement under SEM measurements (Figures S10 and S11, Supporting Information), indicating scanning electronic excitation resulted in similar intermolecular distortions that translate into the movement. These above observations allow us to conclude that the movement direction and behavior of the microscale assemblies can be simply modulated by altering the molecular organization within the microribbon, which can be easily achieved through chemical modification.

In addition, we fabricated microribbons from other PDI molecules (**Figure 6**) with methoxy-substituted phenyl moieties directly linked to the perylene core (molecule **6** and **7**) and investigated their laser-driven movements. No movements were observed in these microribbons, even after the irradiation intensity was increased to 200 W mm^{-2}. We believe that the rigidity of the phenyl groups directly linked to the perylene core restricts the excited-state intermolecular distortion and thus results in no movement. The introduction of a methylene linker increases the flexibility for the excited-state geometric distortion and thus favors the movement of the resulting assemblies, as observed in the cases of molecules **1–4**. To further support this hypothesis, we extended the investigation to PDI molecules with alkyl side chains (Figure 6) that can form similar microribbon morphologies. The alkyl side chains (molecules **8–10**) are more flexible than the phenyl group, and they indeed result in a faster movement of the resulting microribbons, as shown in **Table 1**. Theoretical calculations showed that according to DECM, **8–10** are expected to exhibit longitudinal movement because their HOMO/LOMO distributions support quadrupole–quadrupole interaction, in good agreement with the experimental results, i.e., along the long axis of the microribbon.

In conclusion, we report that the direction-controlled continuous movement of self-assembled microribbons can be achieved using scanning light irradiation as an energy input. We develop a theory of "dynamic exciton charge model" to elucidate that the photoexcited intermolecular distortions create preferred internal motion in between the molecules that in turn spatially translate into an overall directional movement of microribbons. Through chemical modification of side chains of the building block to modulate the diagonal direction of the π-stacks and in turn the diagonal photoexcited distortion relative to the long axis of the microribbon, angular movements of the resulting microribbons were also achieved. Our findings provide an innovative strategy for the design and control of microscale systems capable of continuous and directional movement driven by light, which is distinct from those molecular motor-based systems.

Experimental Section

Detailed synthesis of molecules **1**–**10** and self-assembly of these molecules into the microribbons are described in the Supporting Information.

Movement Measurements: A schematic of imaging of microribbon movement by confocal laser scanning microscopy (CLSM Olympus FV1000) is shown in the Supporting Information. Transmission tunnel images of the microribbons on a surface-modified glass slide were recorded with an Olympus FV1000 inverted confocal laser scanning microscopy coupled with three continuous wave lasers (488, 515, and 635 nm). The laser scanning takes place in a left-right and then top-down direction. The scanning speed of the laser and scanning frame can be set in the range of 2–200 µs per pixel and 800 × 800 pixels, respectively (in specific experiments, different scanning speed and frame

Table 1. Summary of the movement of the microribbons assembled from **1** to **10**.[21]

Microribbon from molecule	Movement velocity*	Movement direction or behavior
1	0.3 ± 0.1 µm min^{-1}	Transversal movement
2	0.7 ± 0.2 µm min^{-1}	Longitudinal movement
3	0.4 ± 0.2 µm min^{-1}	Angular movement
4	0.7 ± 0.1° min^{-1}	Rotational movement
5	1.5 ± 0.3° min^{-1}	Rotational movement
6	–	–
7	–	–
8	2 ± 0.5 µm min^{-1}	Longitudinal movement
9	1.7 ± 0.1 µm min^{-1}	Longitudinal movement
10	1.6 ± 0.2 µm min^{-1}	Longitudinal movement

*For convenient comparision, the laser irradiation mode was set identical (488 nm, 54 W mm^{-2}, 8 µs pixel^{-1}, 700 × 200 pixels per frame).

resolution were used). All images and movies were recorded by CLSM using objective lens (Olympus, UPLSAPO 100 XO; 1.40 NA, 100×). Pictures and movies were processed by Olympus Fluoview software. Their selected area fluorescence spectra were measured on the same apparatus in a XYLamda scanning mode and processed by Olympus Fluoview software.

Time-Resolved Spectral Trajectories Measurements: A nanosecond pulsed laser (532 nm, repetition rate: 1 KHz, pulse duration: 4.5 ns) was used as the pump beam for the photoexcitation of one end of the microribbon. The pump beam was focused to a 10 μm diameter spot using an objective lens (20×, numerical aperture: 0.4). Emission went through the same objective lens and a semi-transparent mirror before the collection by the spectrometer (Andor SR-500i-B2-R) with a resolution of 8 ms. All experiments were carried out at room temperature.

Optical and Structural Characterization: The emission polarization was measured by a custom-built optical microscopy equipped with a 50×, 0.9 NA excitation objective at room temperature in air. Linear dichroism measurement was carried out on an Olympus ix 81 inverted optical microscopy coupled with Olympus polarizer with 0.1° adjustment of polarization direction. Transmission electron microscopy (TEM) images and SAED patterns were obtained with an FEI Tecnai G^2 T20 (120 KV) electron microscopy. XRD measurements were carried out with a Philips X'PertPro instrument (40 KV, 40 mA). SEM measurements were performed with a Hitachi S4800 scanning electron microscopy where the accelerating voltage and the current were set as 10 KV and 10 μA, respectively. UV–vis absorption spectra of the microribbons suspended in ethanol were measured on a PerkinElmer Lamba 35 spectrophotometer.

Theoretical Calculations: A series of density-functional-theory (DFT) calculations to examine optical excitations of molecules **1** and **2** was performed. Ground (G) and excited states (Sn, where n is the order of excitations) of monomers are optimized with the B3LYP functional and the 6–31G* basis set through time-dependent DFT[31–33] method in the Gaussian 09 package which has been successfully used to describe the optical excitation of π-conjugated molecules.[34,35] Based on frontier molecular orbital analysis, it is found that the HOMOs of both molecules are located on the phenyl rings, while the LUMOs located on the PDI core. Because the excitation lifetime is obviously shorter than the molecule movement resonant time scale, it is sufficient to consider only the first excitation states (S1). Thus, electrons transfer from phenyl rings to PDI cores upon excitation, creating one single large dipole on **1** but two opposite small dipoles on **2**.

A "dynamic exciton charge model" to elucidate the excitation-induced instantaneous intermolecular excitonic electrostatic interactions was developed to reveal possible motions of molecules relative to their original π–π stacking structures. For simplicity, the excitonic charge state was represented by placing a positive and negative point charge at the center of phenyl ring and PDI core, respectively. On **1**, the two charges are equal; on **2**, the positive charge is half of the negative one. Then, the electrostatic potential energy is minimized by scanning on a number of crystalline patterns to account for possible molecular motions. A system size from $5 \times 3 \times 3$ up to $50 \times 30 \times 30$ molecules is used, which all give similar results.

Supporting Information

Supporting Information is available from the Wiley Online Library or from the author.

Acknowledgements

This work was supported by 973 project (No. 2013CB632405), NSFC (Grant Nos. 21221002, 21322701, 21577147, and 21590811), the "Strategic Priority Research Program" of the CAS (Grant No. XDA09030200), and the "Youth 1000 Talent Plan" Fund. Utah group thanks support by DOE-BES (Grant No. DE-FG02-04ER46148).

Received: May 6, 2016
Revised: July 12, 2016
Published online: August 15, 2016

[1] W. R. Browne, B. L. Feringa, *Nat. Nanotechnol.* **2006**, *1*, 25.
[2] S. Kobatake, S. Takami, H. Muto, T. Ishikawa, M. Irie, *Nature* **2007**, *446*, 778.
[3] M. Morimoto, M. Irie, *J. Am. Chem. Soc.* **2010**, *132*, 14172.
[4] Y. Nabetani, H. Takamura, Y. Hayasaka, T. Shimada, S. Takagi, H. Tachibana, D. Masui, Z. Tong, H. Inoue, *J. Am. Chem. Soc.* **2011**, *133*, 17130.
[5] Y. Liu, A. H. Flood, P. A. Bonvallet, S. A. Vignon, B. H. Northrop, H.-R. Tseng, J. O. Jeppesen, T. J. Huang, B. Brough, M. Baller, S. Magonov, S. D. Solares, W. A. Goddard, C.-M. Ho, J. F. Stoddart, *J. Am. Chem. Soc.* **2005**, *127*, 9745.
[6] L. Zhu, R. O. Al-Kaysi, C. J. Bardeen, *J. Am. Chem. Soc.* **2011**, *133*, 12569.
[7] T. Kim, L. Zhu, L. J. Mueller, C. J. Bardeen, *J. Am. Chem. Soc.* **2014**, *136*, 6617.
[8] J. Berna, D. A. Leigh, M. Lubomska, S. M. Mendoza, E. M. Perez, P. Rudolf, G. Teobaldi, F. Zerbetto, *Nat. Mater.* **2005**, *4*, 704.
[9] H. Koshima, N. Ojima, H. Uchimoto, *J. Am. Chem. Soc.* **2009**, *131*, 6890.
[10] N. Hosono, T. Kajitani, T. Fukushima, K. Ito, S. Sasaki, M. Takata, T. Aida, *Science* **2010**, *330*, 808.
[11] T. Ikeda, J.-i. Mamiya, Y. Yu, *Angew. Chem. Int. Ed.* **2007**, *46*, 506.
[12] S. Iamsaard, S. J. Asshoff, B. Matt, T. Kudernac, J. J. L. M. Cornelissen, S. P. Fletcher, N. Katsonis, *Nat. Chem.* **2014**, *6*, 229.
[13] M. Yamada, M. Kondo, J.-i. Mamiya, Y. Yu, M. Kinoshita, C. J. Barrett, T. Ikeda, *Angew. Chem. Int. Ed.* **2008**, *47*, 4986.
[14] H. Jiang, S. Kelch, A. Lendlein, *Adv. Mater.* **2006**, *18*, 1471.
[15] C. L. van Oosten, C. W. M. Bastiaansen, D. J. Broer, *Nat. Mater.* **2009**, *8*, 677.
[16] M. Warner, L. Mahadevan, *Phys. Rev. Lett.* **2004**, *92*, 134302/1.
[17] R. Medishetty, A. Husain, Z. Bai, T. Runcevski, E. R. Dinnebier, P. Naumov, J. J. Vittal, *Angew. Chem. Int. Ed.* **2014**, *53*, 5907.
[18] T. Kim, M. K. Al-Muhanna, S. D. Al-Suwaidan, R. O. Al-Kaysi, C. J. Bardeen, *Angew. Chem. Int. Ed.* **2013**, *52*, 6889.
[19] R. Eelkema, M. M. Pollard, J. Vicario, N. Katsonis, B. S. Ramon, C. W. M. Bastiaansen, D. J. Broer, B. L. Feringa, *Nature* **2006**, *440*, 163.
[20] Y. Zhang, C. Peng, Z. Zhou, R. Duan, H. Ji, Y. Che, J. Zhao, *Adv. Mater.* **2015**, *27*, 320.
[21] E. H. Hadicke, F. Graser, *Acta Cryst.* **1986**, *C42*, 189.
[22] J. A. Schuller, S. Karaveli, T. Schiros, K. He, S. Yang, I. Kymissis, J. Shan, R. Zia, *Nat. Nanotechnol.* **2013**, *8*, 271.
[23] J. J. Han, A. D. Shaller, W. Wang, A. D. Q. Li, *J. Am. Chem. Soc.* **2008**, *130*, 6974.
[24] D. Kitagawa, H. Nishi, S. Kobatake, *Angew. Chem. Int. Ed.* **2013**, *52*, 9320.
[25] Y. Sawaa, F. Yeb, K. Urayamaa, T. Takigawaa, V. Gimenez-Pintob, R. L. B. Selingerb, J. V. Selingerb, *Proc. Natl. Acad. Sci. USA* **2011**, *108*, 6364.
[26] Y. Forterre, J. Dumais, *Science* **2011**, *333*, 1715.
[27] S. Armon, E. Efrati, R. Kupferman, E. Sharon, *Science* **2011**, *333*, 1726.
[28] A. Ashkin, *Phys. Rev. Lett.* **1970**, *24*, 156.

[29] M. Burnworth, L. Tang, J. R. Kumpfer, A. J. Duncan, F. L. Beyer, G. L. Fiore, S. J. Rowan, C. Weder, *Nature* **2011**, *472*, 334.
[30] B. Kundys, M. Viret, D. Colson, D. O. Kundys, *Nat. Mater.* **2010**, *9*, 803.
[31] G. Scalmani, M. J. Frisch, B. Mennucci, J. Tomasi, R. Cammi, V. Barone, *J. Chem. Phys.* **2006**, *124*, 094107/1.
[32] M. Chiba, T. Tsuneda, K. Hirao, *J. Chem. Phys.* **2006**, *124*, 144106/1.
[33] M. Caricato, B. Mennucci, J. Tomasi, F. Ingrosso, R. Cammi, S. Corni, G. Scalmani, *J. Chem. Phys.* **2006**, *124*, 124520/1.
[34] A. E. Clark, C. Qin, A. D. Q. Li, *J. Am. Chem. Soc.* **2007**, *129*, 7586.
[35] C. Fang, B. Oruganti, B. Durbeej, *J. Phys. Chem. A* **2014**, *118*, 4157.